water

MDPI

Article

Impact of the Draft Plate on the Wall Erosion and Flow Field Stability of a Cyclone Separator

Yida Zhang [1], Xiaodong Zhang [2,*] and Yanjiao Gao [2]

[1] State Key Laboratory of Complex Nonferrous Metal Resources Clean Utilization, Kunming University of Science and Technology, Kunming 650093, China; zyd200813@163.com
[2] College of Civil Engineering and Architecture, Liaoning University of Technology, Jinzhou 121001, China; tmgyj@lnut.edu.cn
* Correspondence: zhangxiaodong@lnut.edu.cn

Abstract: Cyclone separators are commonly employed in the mining, metallurgy and chemical industries due to their simple structure, easy maintenance and high recovery efficiency. However, with the wide application of cyclone separators, many problems have become exposed in their practical operation, restricting their development. Among these, wall erosion is becoming a significant problem. In this study, to resolve the problem of severe erosion on the walls, the Eulerian–Lagrangian framework was employed to investigate a cyclone separator with a draft plate at the inlet and to evaluate the effect of a draft plate with angles of 0°, 45° and 90° on the degree of erosion and the stabilization of flow fields. Moreover, after verifying the reliability of the numerical model via data from experiments, the characteristics of gas–solid flow were analyzed and the effects of the new structure on the degree of wear were investigated. The results demonstrated that unfavorable phenomena such as secondary flow and wall erosion generated during the operation could be mitigated by the draft plate. When the plate angle was 90°, the wall erosion was the lightest and the range of influence of the secondary flow was the smallest. When the plate angle was 45°, the comprehensive performance was the best, and there was a better balance between the energy loss and the degree of wall erosion. Therefore, the presence of the draft plate has a significant impact on the interaction of gas–solid phases in a cyclone separator.

Keywords: cyclone separator; draft plate; gas–solid phases; computational fluid dynamics; erosion

Citation: Zhang, Y.; Zhang, X.; Gao, Y. Impact of the Draft Plate on the Wall Erosion and Flow Field Stability of a Cyclone Separator. *Water* **2024**, *16*, 3142. https://doi.org/10.3390/w16213142

Academic Editors: Yonggang Lu, Yandong Gu, Yongyao Luo and Wenwu Zhang

Received: 13 October 2024
Revised: 26 October 2024
Accepted: 1 November 2024
Published: 3 November 2024

1. Introduction

Cyclone separators are devices that utilize fluid pressure to generate rotational motion for two-phase and multi-phase separations when there is a difference in density [1]. Due to their relatively low energy consumption, simple structure, recovery efficiency and other advantages, they are widely used in coal-fired, petrochemical, metallurgical and other industrial fields. Although cyclone separators have a simple structure, their separation and trapping processes involve extremely complex three-dimensional multiphase turbulent motion, thus increasing the difficulty of theoretical and experimental research [2]. Nevertheless, studies on cyclone separators have continued to advance over the years. Bogodage et al. [3] explored the capabilities of improved cyclone separators with down-comer tubes (solid loading rate = 0–8.0 g/m^3, inlet velocity = 10 m/s) and revealed that the separation efficiency of particles via down-comers increased when the separated spaces were enlarged and high-tangential-velocity-dominated zones were established. The study by Demir et al. [4] suggested that the pressure drop declined with the enhancement of the body height and conical height, while it increased with the enhancement of the vortex finder height. Furthermore, a modified eddy current detector with a reflux cone and a helical gap was recognized as having good prospects in gas–solid separation in natural gas cleaning [5].

Although much progress has been made regarding detection methods to measure the velocity distribution in the gas–liquid phase, such as in laser Doppler velocimetry (LDV) [6] and particle image velocimetry (PIV) [7], the development of experimental studies has been limited by the equipment's high cost and low measurement efficiency. Currently, with the continuous advances of calculating software, computational fluid dynamics (CFD) is considered to be an effective method for the in-depth exploration and prediction of the flow fields of the separators. Moreover, the Euler–Euler [7] and Euler–Lagrange equations are generally selected as the primary numerical approaches to analyze two-phase gas–solid flows. However, the Euler–Euler method only obtains the overall information of the flow field instead of tracking the position and velocity information [8]. To overcome this drawback, the discrete particle method in the Lagrangian framework (CFD-DPM) has been introduced [9]. The application of this method allows the flow behavior to be addressed from a particle perspective and more comprehensive results to be obtained by tracking the particles. Currently, CFD-DPM is widely used in investigating complex gas–solid turbulent flows in cyclone separators. Duan et al. [10] found that by applying the Euler–Lagrange approach, the resistance time and distance of movement of fine particles in cyclone separators with inner cylinders were extended while eliminating upward and downward flow. Again, applying the Euler–Lagrange formula, Wasilewski et al. [11] investigated cyclone separators with a specific inlet duct bending angle and found that the separation efficiency was limited by the angular margin. Afterwards, Safikhani et al. [12] used the Rosin–Rammler distribution function to inspect the impact of various structural parameters on collection efficiency.

The above studies mainly explored the relationship between structural optimization and flow characteristics such as pressure drop and separation performance. However, it should be emphasized that wall erosion has become a primary problem restricting the application and development of cyclone separators, and few studies have addressed this issue. Specifically, the particles carried by fluids moving at high speeds within the cyclone are highly likely to cause wall erosion, in contrast to other dust removal equipment. Wall erosion directly restricts long-term operation, causing large economic losses to the product [13]. Thiana et al. [14] studied a cyclone separator with fluid catalytic cracking particles as the solid phase and found that erosion increased at velocities of 30 and 35 m/s and decreased with an increasing solid-loading rate. Ehsan et al. [15] explored the effect of inhomogeneous surface roughness on cyclone erosion and found that the erosion rate of particles against inhomogeneous rough walls was less than that of smooth walls. Mohamadali et al. [16] found that the gas flow rate and inlet temperature had the greatest effect on cyclone preheater erosion. Zhang et al. [17] found that as the erosion thickness increases, the pressure drop decreases and the separation efficiency decreases. At the same time, with the increase in local erosion, the phenomenon of fine particles escaping is obvious and the stroke is overlapped, forming a high concentration of the ash ring and intensifying the wear. Zhao et al. [18] proposed a draft plate inner member to improve the separation performance by suppressing the extrusion of the secondary flow with the inlet gas stream. It was found that as the angle of the plate increased, the pressure drop decreased and the separation efficiency decreased. A plate with an angle greater than 90° can substantially reduce the pressure loss, but the prerequisite for using this method is that the separation efficiency is not required to be high. However, the possibility of suppressing the effect of secondary return flow through the plate and thus influencing the internal flow field to regulate erosion is a question that deserves investigation.

Therefore, the study of the variation in the degree of erosion is essential to determine the optimum angle of the plate to improve cyclone operation [19]. Meanwhile, CFD-based erosion calculation models are another powerful tool in addition to experiments to provide an in-depth understanding of complex turbulent flows and the calculation of wear.

Based on the discussion above, this study focused on the effect of plates and their angles on the degree of erosion, flow field characteristics and particle behavior using the Eulerian–Lagrangian method. Firstly, the two-phase gas–solid flow pattern under

the influence of the plate was presented, the distribution of the gas-phase velocity was investigated and the pressure drop was calculated. Secondly, particle trajectories were investigated in systems with and without draft plates and emphasis was placed on the effect of the plate on the degree of erosion on the walls. Finally, the interaction between the wall wear and the location of swirls and vortex nuclei in the flow field was further analyzed. This study aims to provide a comprehensive understanding of the complex interactions among the gas phase, particles and the body of the device with the addition of a plate.

2. Computational Method

2.1. Governing Equations of Liquids

The universal turbulence model used in this study is the Reynolds stress model, in which the eddy viscosity assumption is circumvented and each component of the Reynolds stress tensor is calculated. The directional effects of Reynolds stress and complex interactions in turbulence are also explained. The Reynolds stress model is appropriate for considering the effects of rotational flow and changes in surface curvature in the direction of flow. In this study, response surface methodology (RSM) was applied to simulate the gas phase [14,20,21], which was assumed to be incompressible and isothermal. The continuity and Reynolds-averaged Navier–Stokes equations are depicted in Equation (1) and Equation (2). The transport equation of Reynolds stresses is presented in Equation (3). The molecular diffusion term is defined based on Equation (4), where μ_t is the turbulent viscosity with coefficient σ_k = 0.82. The buoyancy generation term is calculated using Equation (5). In Equation (5), T is the temperature, Pr_t refers to the turbulent *Prandtl* number of energy (in this model, Pr_t = 0.85), g_i is the component of the acceleration of gravity in the *ith* direction and β represents the coefficient of thermal expansion. The dissipation term refers to the dissipation of *Reynolds* stress by molecular viscosity. In establishing the equation for the dissipation term, it is assumed that the large-scale vortices are responsible for the kinetic energy transport and the small-scale vortices are responsible for the viscous dissipation, and therefore the small-scale vortex clusters can each be viewed as isotropic. Following this assumption, the dissipation term can eventually be expressed in Equation (6), and where Y_M is an additional diffusion term, it can be solved according to Equation (7).

$$\frac{\partial \overline{u}_i}{\partial x_i} = 0 \tag{1}$$

$$\frac{\partial \overline{u}_i}{\partial t} + \overline{u}_i \frac{\partial \overline{u}_i}{\partial x_j} = -\frac{1}{\rho}\frac{\partial \overline{p}}{\partial x_i} + v\frac{\partial^2 \overline{u}_i}{\partial x_i \partial x_j} - \frac{\partial}{\partial x_j} R_{ij} \tag{2}$$

$$\frac{\partial\left(\rho u_i' \overline{u}_j'\right)}{\partial t} + \frac{\partial\left(\rho u_k u_i' \overline{u}_j'\right)}{\partial x_k} = D_{ij} + G_{ij} + \phi_{ij} - \varepsilon_{ij} \tag{3}$$

$$D_{ij} = \frac{\partial}{\partial x_k}\left(\frac{\mu_t}{\sigma_k}\frac{\partial u_i' \overline{u}_j'}{\partial x_k}\right) \tag{4}$$

$$G_{ij} = \beta\frac{\mu_t}{Pr_t}\left(g_i\frac{\partial T}{\partial x_j} + g_i\frac{\partial T}{\partial x_i}\right) \tag{5}$$

$$\varepsilon_{ij} = \frac{2}{3}\delta_{ij}(\rho\varepsilon + Y_M) \tag{6}$$

$$Y_M = 2\rho\varepsilon M_t^2 \tag{7}$$

2.2. Governing Equations of Solids

The Euler–Lagrange method is commonly used to track solid particles because of its ability to accurately capture particle trajectories. In this study, the Eulerian–Lagrangian method is employed to analyze the phase motion of the particles. Newton's second law (Equation (8)) is utilized to track the motion of the particles. In Equation (8), m_p represents

the particle mass. Assuming that the particles are spherical, only the gravity and drag force are considered. The equation for particle motion is defined as in Equation (9) and Equation (10), where $\vec{F}_d$ is the drag force, $\vec{F}_l$ represents the lift force, $\vec{F}_g$ represents the gravitational force, $\vec{F}_m$ is the virtual mass force, $\vec{F}_{pre}$ refers to the pressure-gradient force, $\vec{F}_c$ is the collision force of the particle–particle/wall, $\vec{u}$ is the fluid phase velocity and $\vec{u}_p$ denotes the particle velocity. Additionally, particle relaxation time τ_r is exhibited in Equation (11). Here, ρ_p represents the density of the particle, d_p is the particle diameter and Re is the relative Reynolds number, as shown in Equation (12). A drag coefficient of C_D = 0.405 is assumed for spherical particles. This drag coefficient, C_D, for spherical particles is presented in Equation (13), where a_1, a_2, and a_3 are constants applied over several ranges of Re, as proposed by Morsi and Alexander [19].

$$m_p \frac{d\vec{u}_p}{dt} = \vec{F}_p \tag{8}$$

$$\vec{F}_p = \vec{F}_d + \vec{F}_l + \vec{F}_g + \vec{F}_m + \vec{F}_{pre} + \vec{F}_c \tag{9}$$

$$\frac{d\vec{u}_p}{dt} = \frac{\vec{u} - \vec{u}_p}{\tau_r} + \frac{\vec{g}(\rho_p - \rho)}{\rho_p} \tag{10}$$

$$\tau_r = \frac{\rho_p d_p^2}{18\mu} \frac{24}{C_D Re} \tag{11}$$

$$Re = \frac{\rho_p d_p \left| \vec{u}_p - \vec{u} \right|}{\mu} \tag{12}$$

$$C_D = a_1 + \frac{a_2}{Re} + \frac{a_3}{Re^2} \tag{13}$$

2.3. Erosion Modeling

Wall erosion is caused by particle–wall collisions. Finnie, McLaury, General [22] and Oka [13] erosion models can properly simulate wall erosion. Among them, the McLaury model is more widely used but has been adapted to a smaller interval of particle collision velocities. The Finnie model can relate the erosion rate to the kinetic energy of particles impacting the wall and is more applicable to the calculation of erosion in sand and gravel. In this investigation, the Finnie model is applied to model erosion. The Finnie model is shown in Equation (14), in which k refers to the model constant, V_p represents the impact velocity of the particle and $f(a)$ denotes the function of the impact angle, which can be defined as shown in Equation (15).

$$E = kV_p^n f(a) \tag{14}$$

$$f(a) = \begin{cases} \frac{1}{3}\cos^2 \alpha & \alpha > 18.5^\circ \\ \sin(2\alpha) - 3\sin^2 \alpha & \alpha \leq 18.5^\circ \end{cases} \tag{15}$$

3. Numerical Method and Settings

3.1. Numerical Settings

Figure 1a demonstrates the geometry of a cyclone separator with specific dimensions, as shown in Table 1. In this study, four kinds of draft plates were added to the conventional separator, and the specific morphology and placement are shown in Figure 1b. Here, the Case 1 draft plate has a 0° angle tangential to the wall and is a circular arc surface; the Case 2 draft plate has a 45° angle tangential to the wall and is a moment surface; the Case 3 draft plate has a 90° angle tangential to the wall and is a moment surface; and Case 4 is the traditional cyclone separator. The focus of this study is on the combined impact of various

angle draft plates on the cyclone separator pressure drop, degree of erosion and scope of impact of secondary streams [23].

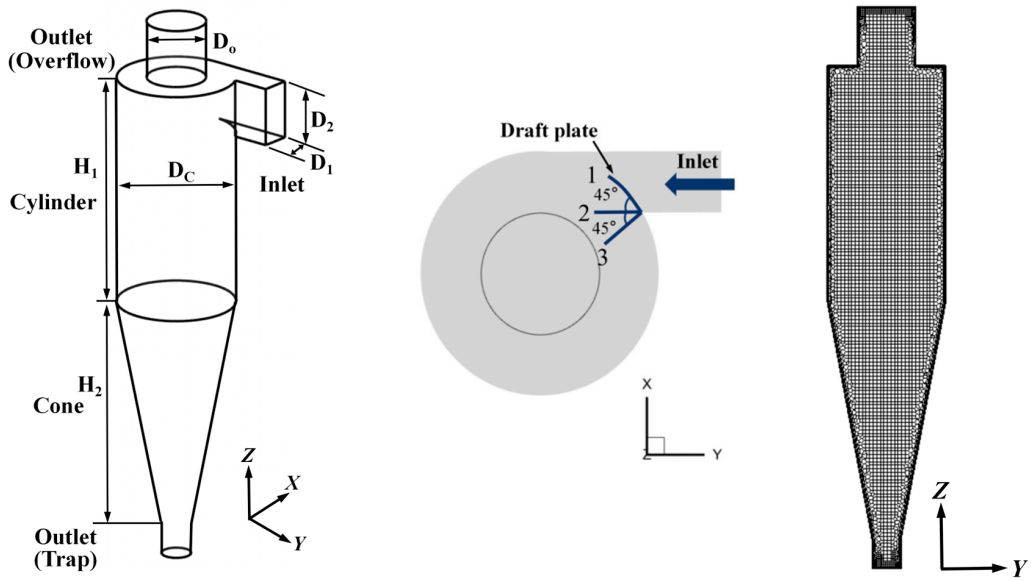

Figure 1. Schematic diagram (**a**), the illustration of the three draft plates on the cyclone separator (**b**) and the grid system generation (**c**).

Table 1. Dimensions of the cyclone separator considered (unit: m).

D_o	D_c	D_1	D_2	H_1	H_2	D_u
0.1	0.2	0.05	0.1	0.4	0.4	0.05

The solid phase in this study is in the shape of a round sphere, designated as a discrete phase, and the particles are released and tracked through the discrete phase model (DPM) [17]. Carbon particles were chosen as the solid phase; the minimum particle diameter was 0.01 mm, and the maximum diameter was 0.1 mm, and the spread parameter was 3.5 [24]. The inlet flow rate was set to 5×10^{-5} kg/s, and the inlet velocities were 20 m/s, 25 m/s and 30 m/s. In this study, gas velocities are consistent with the particle inlet velocities. The number of dividing meshes in Cases 1–4 is about 120,000, where the maximum mesh is 12 mm and the minimum mesh is 1.5 mm.

3.2. Model Validation

3.2.1. Model Validation I

In order to assess the ability of the developed model to predict the gas-phase flow field, the cyclone separator from a previous study [25] was reconstructed and simulated. The model used the same cyclone separator as in the previous study, with an inlet length of 0.05 m, a width of 0.1 m, an overflow diameter of 0.1 m, a dust discharge diameter of 0.05 m, a length of 0.8 m and contained a grid of about 172,146 cells. The grain density was set to 3320 kg/m^3, with an average diameter of 29.9 μm. This study assumed that the inlet velocity was equal to the fluid velocity. The inlet was set as the velocity inlet and the overflow and trap ports were set as the pressure outlets. To couple pressure and velocity, the SIMPLE algorithm was chosen. The pressure drop in this validation was calculated as the difference in pressure between the inlet and the outlet of the overflow. Figure 2 shows the predicted separator pressure drop from the simulation and experimental measurements [25]. It can be seen that the experimental data agreed very well with the numerical data.

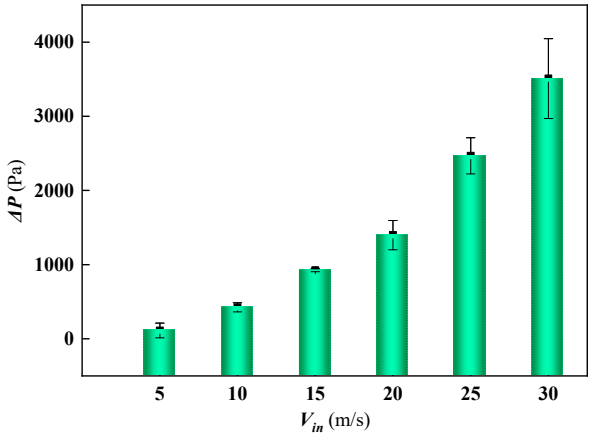

Figure 2. Comparison of the pressure drop between the experiment and the current simulation.

3.2.2. Model Validation II

To verify the validity of the numerical parameters adopted for the solid phase, a literature-complete CFD-DPM simulation is required. The model was the same as the validation one; its dimensional details were mentioned in Section 3.2.1. The cyclone separator contained a total of 3,001,689 cell grids. The gas phase consisted of compressible air with a minimum particle diameter of 67.5 µm, a maximum diameter of 678.5 µm, an average diameter of 263.9 µm and a density of 2300 kg/m^3. The inlet velocity was 2.7 m/s, and the mass flow rate was 1.19 kg/s. The boundary condition settings were consistent with validation I. Figure 3 shows a quantitative comparison of the separation efficiency obtained from the numerical results of the developed model with the experimental results [25]. The equation for the separation efficiency can be expressed in Equation (16). It can be seen from Figure 3 that the experimental data are in good agreement with the numerical data.

$$\eta = \frac{w_{p,inlet} - w_{p,overflow}}{w_{p,inlet}} \times 100\% \quad (16)$$

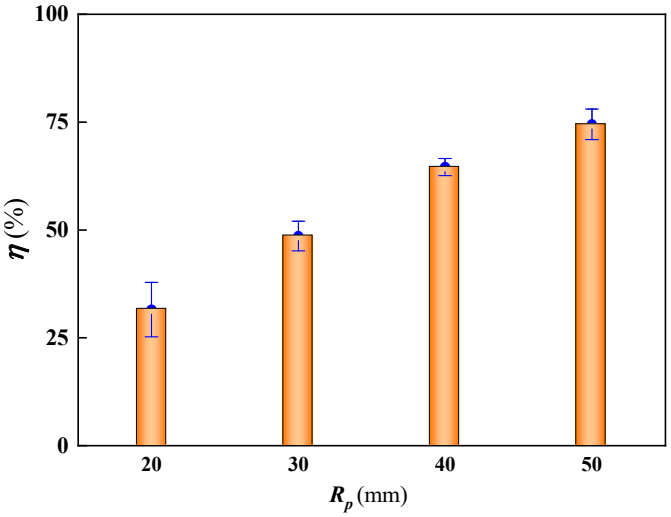

Figure 3. Comparison of separation efficiency between the experiment and the current simulation.

4. Results and Discussion

4.1. Gas Flow Field Characteristics

4.1.1. Tangential Velocity of the Gas Phase

Figure 4 shows the tangential velocity distribution at different heights for different angle plates. The greater degree of symmetry in the tangential velocity was symmetric,

but not perfectly symmetric, due to the presence of a large rotational curvature. The draft plate with the angle of 0° increased the tangential velocity in the flow field to a greater extent than conventional separators. The tangential velocity was suppressed at plate angles greater than 45°. A tangential velocity maximum existed at the junction of the forced and free vortices, and the location of its tangential velocity maximum was the radius of the forced vortex, and the outer side was the free vortex. The quasi-free vortex region was the place where solid particles were detached from the gas stream, and the increase in the free vortex region was conducive to improving the separation efficiency of the separator. Table 2 indicates the radius of the forced vortex of the cyclone separator versus the region of the quasi-free vortex. Case 1 had the largest forced vortex radius, i.e., the smallest region of quasi-free vortices, and the particles rotated more in the gas stream and had poorer separation performance. The forced vortex of Cases 2 and 3 were reduced compared to that of Case 4, and the quasi-free vortex region was reduced, indicating that the separation performance of the separator with a draft plate angle greater than 45° was improved compared to the conventional separator.

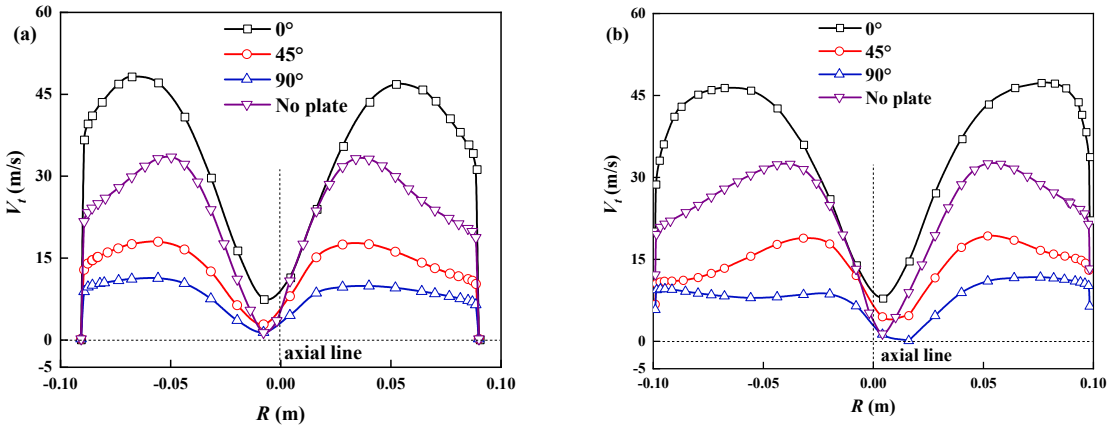

Figure 4. The tangential velocity distribution with draft plates of 0.8 H (**a**) and 0.4 H (**b**).

Table 2. The lengths of the forced vortex and free vortex.

L (m)	Case 1	Case 2	Case 3	Case 4
Forced vortex	0.061	0.045	0.045	0.046
Free vortex	0.029	0.045	0.045	0.044

4.1.2. Pressure Drop

Figure 5 illustrates the impact of different inlet velocities on the pressure drop in the case of the plate. Static pressure is the pressure of the fluid and dynamic pressure is the pressure exerted on the particles. The top half of Figure 5 shows the static pressure drop of the separator, and the bottom half shows its dynamic pressure drop. Compared to the conventional cyclone separator, the static pressure drop in Case 1 was elevated by 2631 Pa and the dynamic pressure drop was elevated by 1 Pa. This indicated that the conversion between static and dynamic pressure in Case 1 was poor and the flow stability would be reduced. Case 2 had a static pressure drop of 1151 Pa and a dynamic pressure drop of 213 Pa, indicating that a larger portion of the static pressure was converted to dynamic pressure. The static pressure drop of Case 3 was 136 Pa, and the absolute value of the dynamic pressure drop was 98 Pa higher compared to Case 2, which indicated that it had a strong ability to convert static pressure to dynamic pressure and consumed less energy. More translational pressure meant greater centrifugal force on the particles. At the same time, the change in inlet velocity had a small effect on the pressure drop. The change in pressure drop was more pronounced when the plate angle was 45°, indicating that it was

more sensitive to the inlet velocity. When the plate angle was 90°, the dynamic and static pressure drops were almost independent of the inlet velocity.

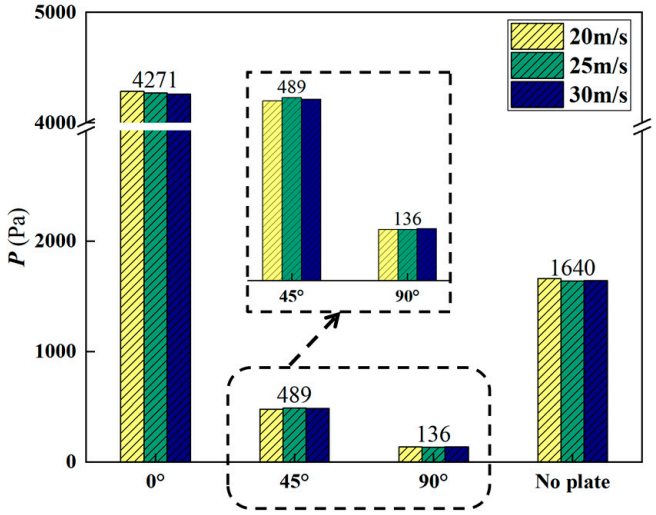

Figure 5. The pressure drop with draft plates under different inlet velocities.

Figure 6 illustrates the pressure distribution for different draft plate cases. The zero-pressure zones with a pressure of 0 Pa at the centers of Cases 1 and 4 were more uniformly distributed in an oscillating cylinder. The zero-pressure zones of Cases 2 and 3 were distributed in the overflow and dust collection ports, with less distribution in the middle of the separator. Case 3 had the lowest overall pressure, and Case 2 had a significant overall pressure gradient. It was shown that the energy loss was significantly reduced when the draft plate angle was greater than 45°. Based on the distribution of the pressure drop and the pressure, as the angle of the plate increased, the static pressure drop decreased and a large amount of the static pressure converted to dynamic pressure, improving the performance even further.

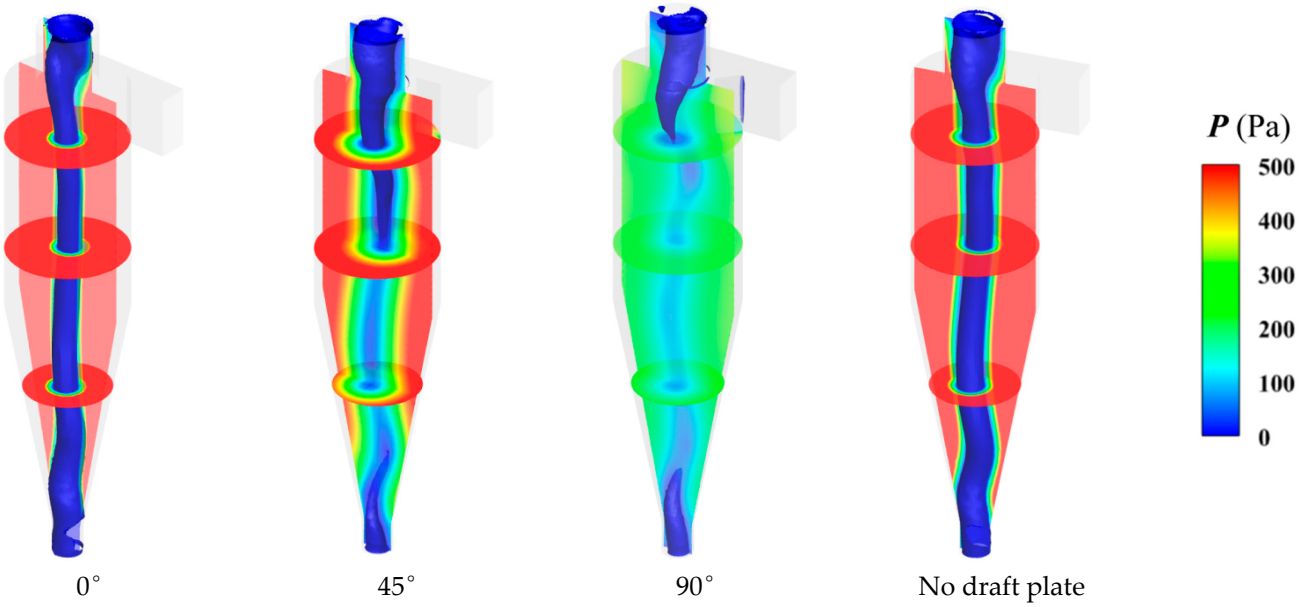

Figure 6. The pressure distribution with draft plates.

4.2. Trajectories of Different-Diameter Particles

Figure 7 shows the particle trajectories for different draft plate cases. In this study, the particles were divided into two groups: larger than 0.01 mm and smaller than 0.01 mm. The

distribution of the particles in Case 1 was more uniform, and the large and small particles rotated in the separator in a spiral shape with a regular trajectory. Compared with the conventional separator, the draft plate with an angle of 0° had a lower degree of obstruction to the particles and had a better effect on adjusting the trajectory of the particles. Case 2 had a small portion of large particles in the cylinder undergoing an irregular helical motion. As can be seen from Figure 3, the tangential velocity of Case 2 was reduced, and thus the wall-touching ability was reduced, which increased the angle at which the particles wrapped around the separator. At the same time, the overflow of small particles was larger than that of Case 1. Due to the variation in its large and small particles, it was inferred that Case 2 had a lower separation efficiency. Under the influence of the draft plate, the particles of Case 3 as a whole showed an upward drift. Among them, the large particles were more affected by the draft plate, only a small portion of them were collected by the dust collection port and most of them rotated in the cylinder portion, which increased the possibility of overflowing the separator. Therefore, it was presumed that the overall separation efficiency was reduced. Compared with the traditional separator, the obstruction of particles was weaker when the angle of the draft plate was less than 45°, the trajectory of the particles was mainly in the form of a spiral and the internal flow field was more organized.

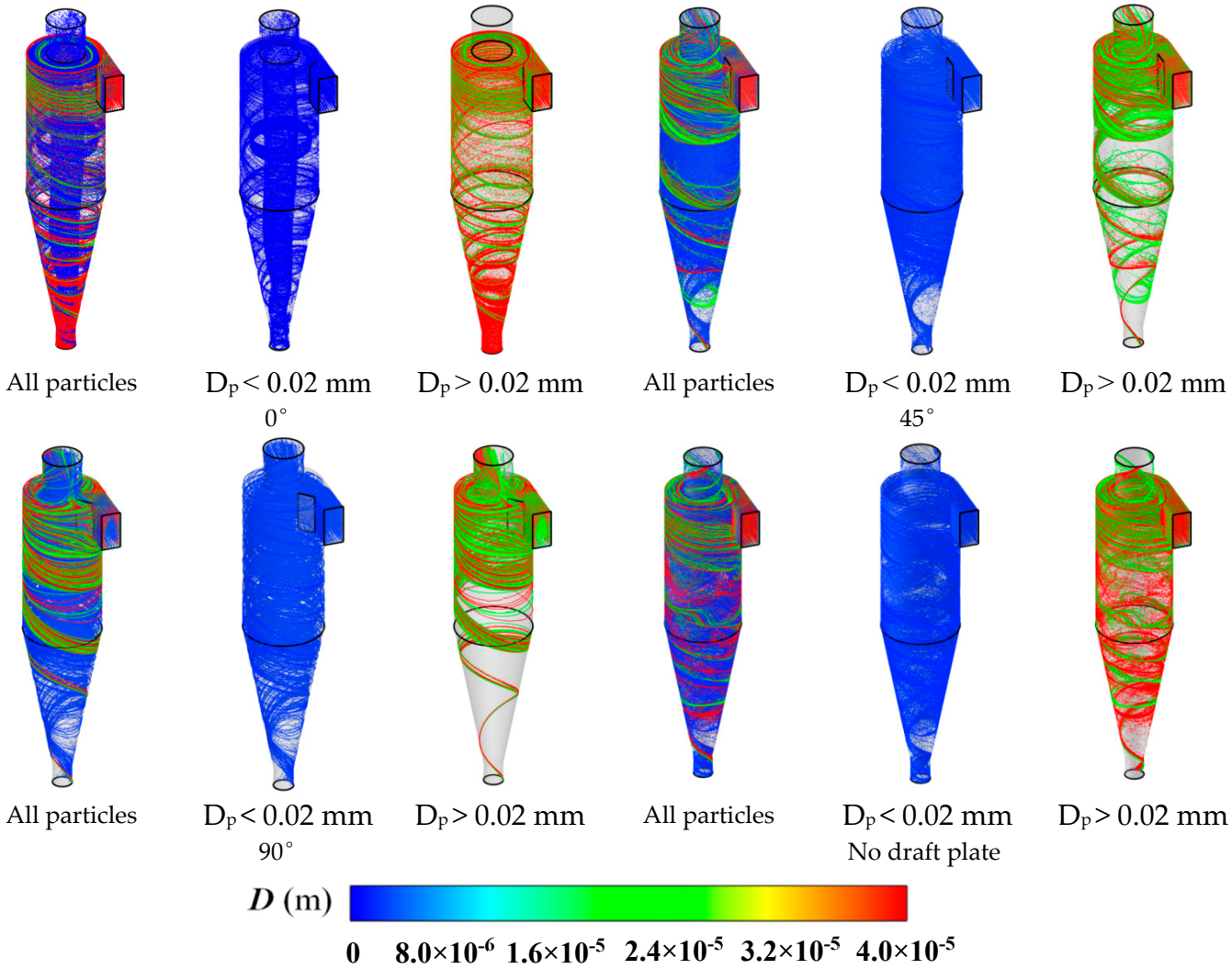

Figure 7. The particle distribution of different diameters with draft plates in the cyclone separator.

4.3. Wall Erosion

Figure 8 exhibits the variation in cyclone wall erosion with three kinds of plate angle. The erosion on the cyclone wall was not uniform over a large area due to particle action, but

rather localized areas were subjected to particle beam erosion. The erosion was significantly more severe in areas where particles were concentrated. At the same time, some areas stored scattered particles, so the cylinder was almost not subject to erosion, with non-uniformity. In Case 1, the cylinder and cone portions were obviously subjected to greater erosion and the entire cone was severely eroded. This indicated that the draft plate with an angle of 0° was less resistant to erosion and presented severe erosion due to the increased tangential velocity. Compared to the case without the plate (Case 4), the erosion area in Case 2 was mainly concentrated at the cone particle ring, with less wear in other areas. This was due to the fact that under the influence of the plate at an angle of 45° (Case 2), the gas streams were less squeezed and collided with each other, and the solid particles carried by them gained less momentum from the gas streams, reducing their ability to collide with the wall of the separator, and thus the erosion rate was lower. Case 3 was overall subjected to the least amount of erosion, with a concentration of erosion occurring only in the upper part of the cylinders and in the dust collection ports. This is due to the reduced tangential velocity of the gas phase in Case 3, as the particles were therefore subjected to lower centrifugal forces and reduced dynamics. The intensity of particle–wall collisions and the overall erosion were reduced.

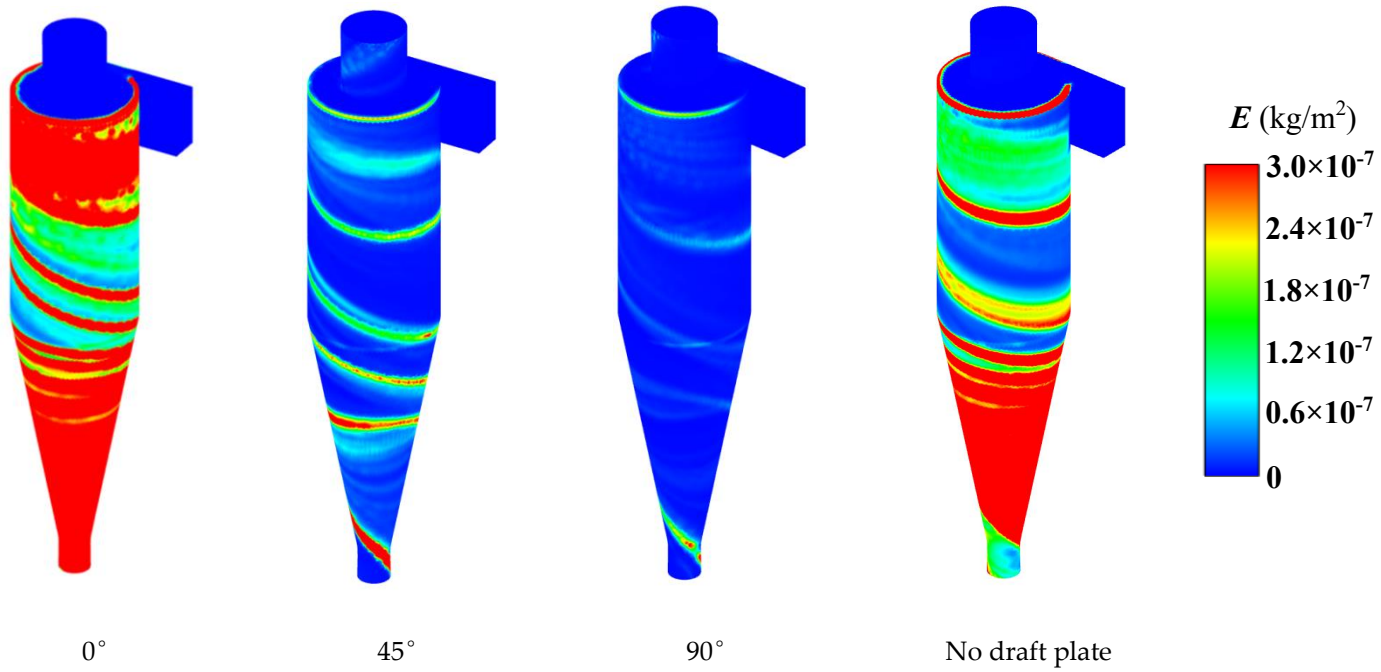

Figure 8. Wall erosion with the draft plates.

Figure 9 illustrates the degree of erosion on the top plate for different draft plates. The erosion on the top plate was related to the flow characteristics of the gas–solid two-phase flow in the corresponding area. The degree of erosion increased with an increasing radius, and the main erosion areas were concentrated between 30° and 300°, with the most severe wear at 80°–200°. Near the top plate of the separator, the particles were subjected to almost equal gravity, resistance, traction and centrifugal force, and thus the particles oscillated and rotated, forming a "top ash ring", the existence of which caused the most serious wear in this area. Cases 1 and 4 had the largest areas of erosion, with more severe erosion from around 30° to 360°. In Case 2, most of the top plate was eroded, while in Case 3 only a small portion of the top plate was eroded. The erosion in Cases 1 and 3 on the inlet wall area was primarily influenced by the inlet airflow.

Figure 10 illustrates the comparison of the degrees of erosion suffered by the cone and cylinder sections for different angles of the plate. As can be seen in Figure 10, the cone section suffered more severe erosion compared to the cylinder section. This was due

to the fact that the rotating vortex nucleus oscillated more at the bottom of the cone, in a non-stationary torsional oscillation phenomenon. The turbulence was more intense in this region and the particles had higher kinetic energy. At an angle of 0°, the difference in erosion between the conical and cylindrical parts was greater. At a draft plate angle of 90°, the overall erosion was more even. The separator with the draft plate was subjected to different degrees of erosion at different inlet velocities. At an angle of 0°, the difference in erosion between the conical and cylindrical parts was greater. At a draft plate angle of 90°, the overall erosion of the wall was more uniform.

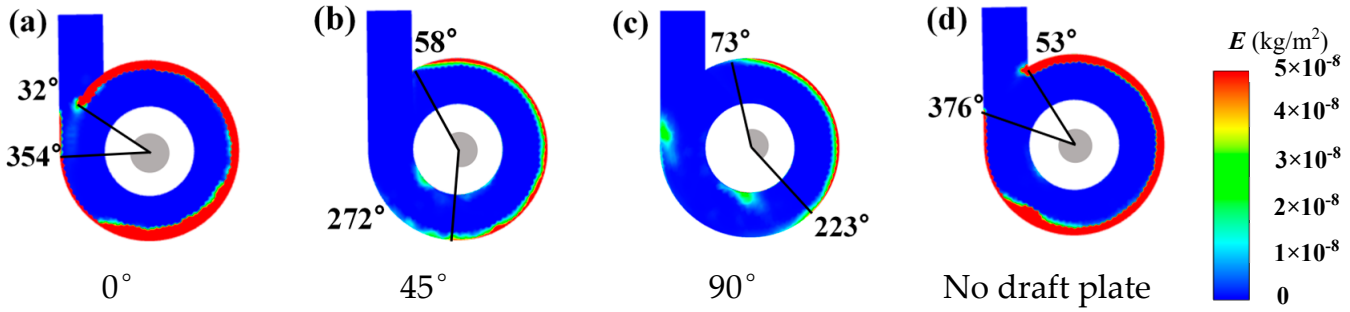

Figure 9. The erosion degree and the angle of the roof with the draft plates. [(**a**): the angle of the plate of 0°;(**b**): the angle of the plate of 45°; (**c**): the angle of the plate of 90°; (**d**): cyclone without plate].

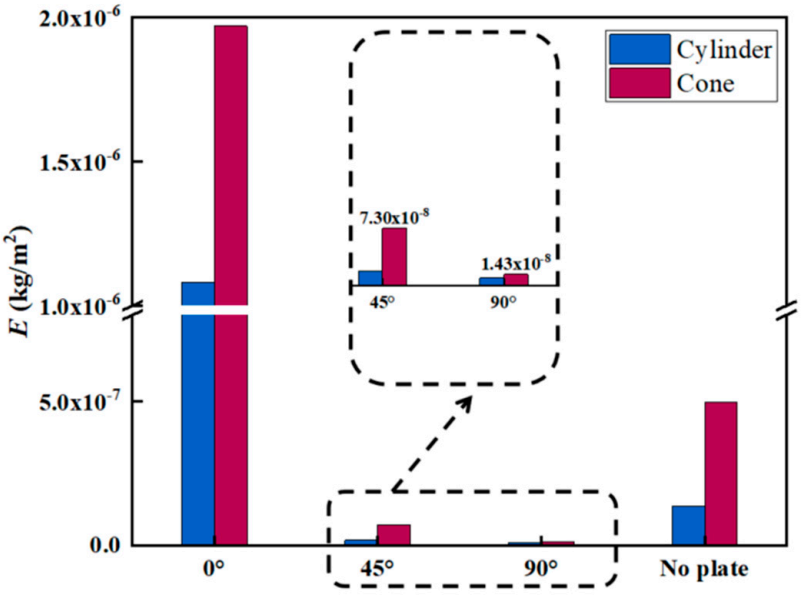

Figure 10. The erosion of the cylinder and cone with the draft plates.

The inlet velocity had a significant effect on the tangential velocity, which further affected the degree of erosion. Tables 3 and 4 show the variation in erosion on the cylinder and cone portions of the cyclone at different inlet velocities. When the inlet velocity was 30 m/s, the overall abrasion suffered was less. When the draft plate angle was 90°, the change in inlet velocity had a greater effect on the degree of wear on the cylindrical section. The change in inlet velocity had almost no effect on the cylindrical part of the separator with a draft plate angle of 45°. With a draft plate angle of 0°, the cone was more sensitive to the inlet velocity and the degree of erosion was more variable. The wear degree of the conventional separator was less affected by the inlet velocity. This indicated that the presence of the draft plate had some influence on the particle motion and internal flow field, resulting in the wear degree being more sensitive to the inlet velocity.

Table 3. The erosion rate of the cylinder.

Erosion (kg/m^2)	Case 1	Case 2	Case 3	Case 4
20 m/s	1.08×10^{-6}	1.89×10^{-8}	9.8×10^{-9}	1.36×10^{-7}
25 m/s	9.07×10^{-7}	1.91×10^{-8}	1.11×10^{-6}	1.36×10^{-7}
30 m/s	9.01×10^{-7}	1.58×10^{-8}	5.48×10^{-7}	1.36×10^{-7}

Table 4. The erosion rate of the cone.

Erosion (kg/m^2)	Case 1	Case 2	Case 3	Case 4
20 m/s	1.97×10^{-6}	7.3×10^{-8}	1.43×10^{-8}	4.98×10^{-7}
25 m/s	7.32×10^{-8}	7.32×10^{-8}	1.49×10^{-8}	4.99×10^{-7}
30 m/s	9.01×10^{-7}	6.35×10^{-8}	5.88×10^{-9}	4.99×10^{-7}

4.4. Separation Efficiency

Figure 11 exhibits the separation performance with various inlet velocities for different plates. Case 1 shows an increased separation efficiency with the plate. Cases 2 and 3 had decreased separation efficiency with the inhibition of the plate. This was due to the fact that the tangential velocity was weakened when the plate was angled at 45° or 90°, and therefore the separation efficiency was reduced.

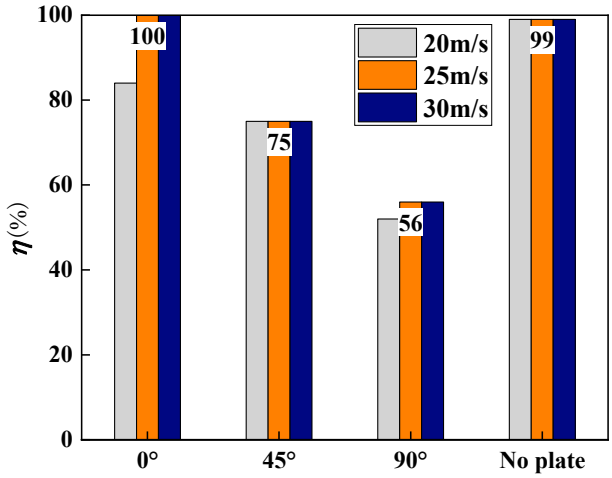

Figure 11. The separation efficiency with draft plates.

Cases 1 and 3 were affected by inlet velocity to a greater extent, and the separation efficiency increased significantly with the increasing inlet velocity. This indicated that plates with angles of 0° and 90° were more sensitive to the inlet velocity. Case 1 is suitable for environments where there is a need to save money and where high separation efficiencies are required along with high gas velocities. When the inlet velocity of the conventional separator was gradually increased from 20 m/s to 30 m/s, the separation efficiency did not change significantly. Case 2 had the same trend as that of the conventional separator, indicating that a large or small angle of the draft plate changed the sensitivity of the internal flow field to the inlet velocity. Case 2 was highly adaptable to different gas velocities and could maintain good separation efficiency up to inlet velocities of 20–30 m/s.

The separation efficiency decreased with the increase in localized erosion, and as can be seen in Figure 8, Case 3 suffered the least amount of erosion, but its separation efficiency was also the lowest, indicating that the magnitude of the tangential velocity had a greater effect on the separation efficiency. Case 3 applies in situations where a significant reduction in resistance is required and where the economic requirements are high but the separation efficiency is not so high. At the same time, Case 3 can apply to high-gas-velocity environments, balancing lower separation efficiencies. Specifically, the decrease in localized

wear improved the separation performance, but the tangential velocity of the gas phase decreased due to the hindering effect of the draft plate, and thus the number of wall touches decreased, leading to a decrease in the separation efficiency. Similarly, Case 1 suffered the most wear, but the separation efficiency was effectively improved due to its maximum tangential velocity.

4.5. Vortex and Vortex Nuclei

Figure 12 illustrates the streamlines in the longitudinal section of the cyclone separator for various angles of the plate. In the cyclone separator, apart from the prevailing inward and outward vortices, there are also secondary flows caused by the interaction of axial and radial velocities. In Figure 12, the vortices are more widely distributed and the area affected by the secondary flow has increased. This is due to the strong abrasion in Case 1, which led to its more unstable flow field. Case 1 was similar to the conventional separator in terms of wear and tear, and therefore the area of the vortex was similar. Case 2 was also subjected to severe erosion; as seen in Figure 12, the localized vortex was larger than the radius of the device and had a large area of influence, resulting in the oscillation of the internal and external vortices, affecting the stability of the flow field. Case 3 was subjected to the least amount of wear and tear, and the localized vortex was concentrated in the middle of the separator, which had a small area of influence; therefore, the vortex had the lowest influence on the flow field. The influence of the vortex on the flow field was minimized. It can be concluded that the degree of erosion on the separator affected the strength of the vortex and the flow field.

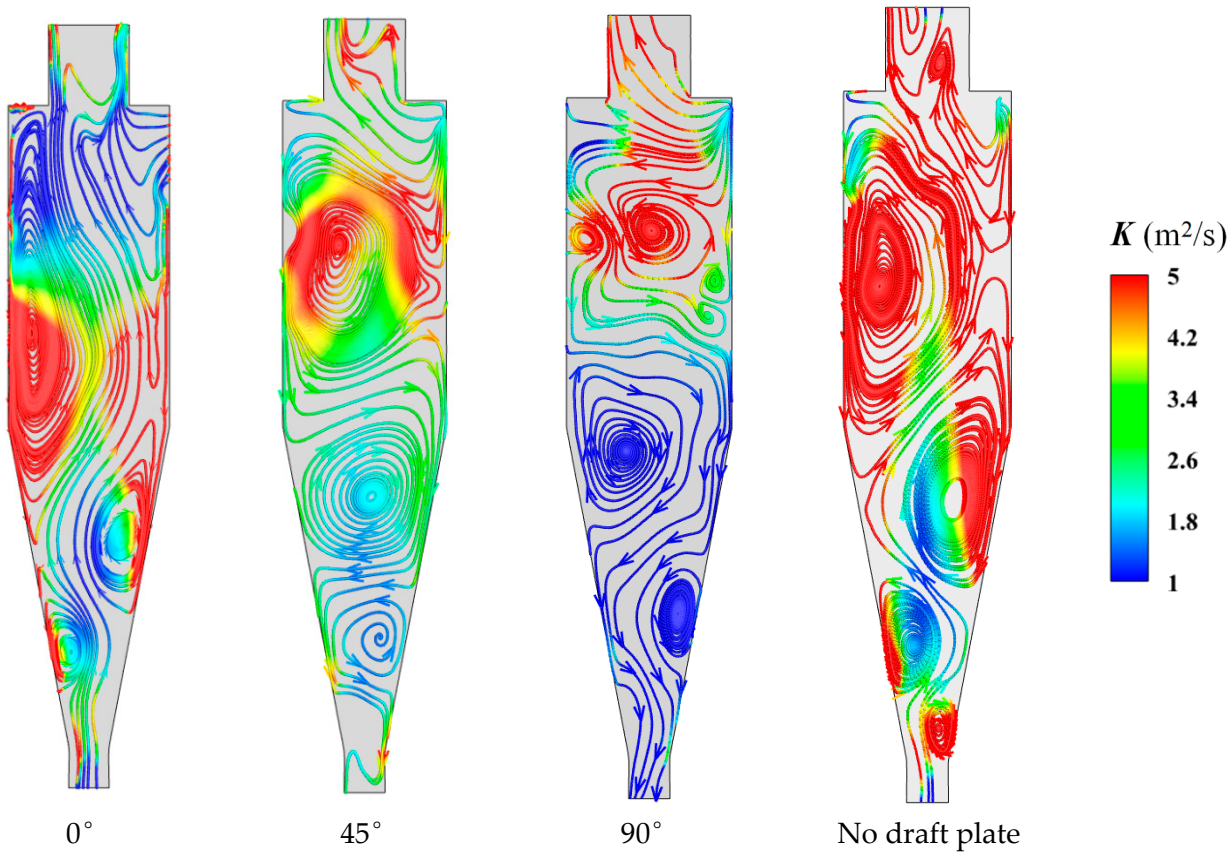

Figure 12. The streamlines of sections with draft plates.

Figure 13 demonstrates the deflection of the vortex core center for different axial positions. The vortex core displacements under different angles of the plate are counted in Figure 14. The vortex core displacement was greater for Cases 2 and 3 and smaller for Case 1. The increase in wall erosion disrupted the internal airflow and increased the displacement

of the vortex core deviation. From Figure 13, it can be seen that as the angle of the plate increased, the degree of erosion decreased, but the vortex core displacement increased, indicating that the process of changing the vortex core position was more complicated and was not only related to the degree of wear. At the same time, the vortex core displacement also had a strong relationship with the tangential velocity. Specifically, the vortex core formed a region between the vortex core and the center of the ensemble surrounded by a zero-tangential velocity envelope, so that a decrease in vortex core displacement increased the tangential velocity.

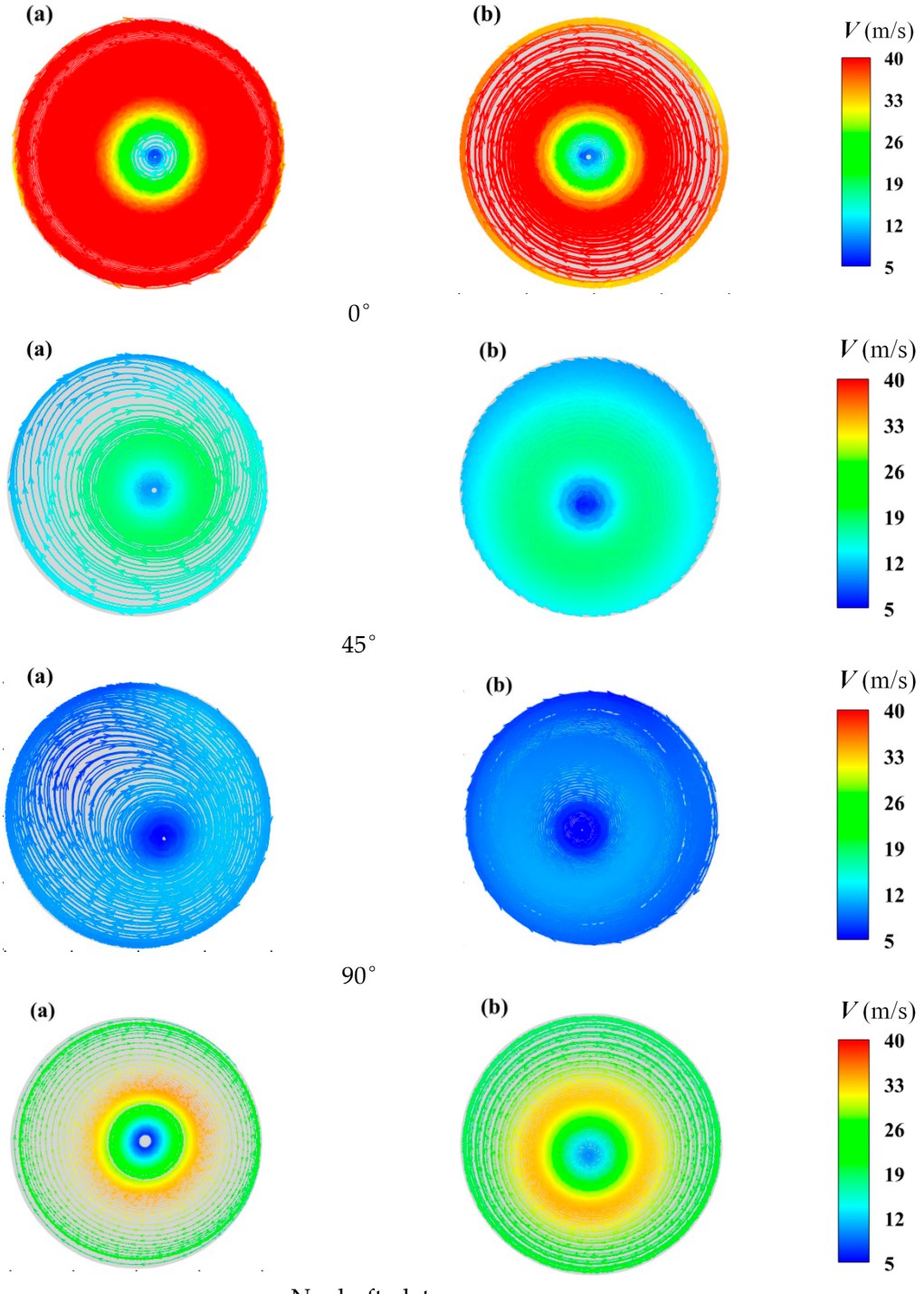

Figure 13. The streamlines $Z/H = 0.75$ (**a**) and $Z/H = 0.6$ (**b**) with draft plates.

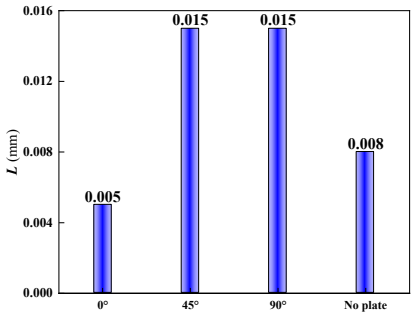

Figure 14. The deviation displacement of the vortex core (unit: mm).

Case 1 had the highest intensity of localized eddy currents, which was due to the fact that it was subjected to stronger localized wear. Cases 2 and 3 reduced the intensity of the localized eddy currents due to having less wear.

5. Conclusions

In this study, the Euler–Lagrange method was employed to simulate the two-phase gas–solid flow in a cyclone separator with draft plates, and the effects of different draft plate angles on the flow characteristics (e.g., velocity, dynamic pressure and static pressure), particle behavior and the degree of erosion were discussed. The main results of this study were as follows.

(1) The presence of the draft plate significantly affected the movement of gas and particles. Increasing the angle of the draft plate effectively suppressed the compression of the inlet gas flow via the gyrating one-week gas flow, which reduced the pressure drop of conventional separators by 92%, improved the ability to rotate the pressure at static pressure and reduced energy consumption.

(2) Increasing the angle of the draft plate reduced the gas-phase flow field dynamics, leading to a reduction in the tangential velocity and effectively controlling the erosion phenomenon on the cyclone wall. Due to the larger swing of the spinning-in vortex nucleus at the bottom of the cone, the turbulence was more intense and the cone part of the cyclone separator was subjected to more serious erosion than the cylinder part.

(3) The existence of the plate improved the stability of the flow field while weakening the erosion of the cyclone wall. Due to the interactions of the wall, particles and the internal flow field, the local vortex area of the separator was minimized when the plate angle was 90°, which minimized the scope of influence on the internal secondary flow.

Current research has greatly reduced the energy loss and wall wear of cyclone separators, but there has been a lack of exploration of particle breakage and binding. Future research will be devoted to the study of individual particle behavior, which will be beneficial to the design and optimization of these systems.

Author Contributions: Conceptualization, Methodology, Software and Writing—Original Draft, Y.Z.; Writing—Review and Editing, X.Z.; Formal analysis and Supervision, Y.G. All authors have read and agreed to the published version of the manuscript.

Funding: This study was financially supported by Yingkou Hengdong Water Conservancy Service Co. (Heng 20230210) and the 2024 Fundamental Research Funding of the Educational Department of Liaoning Province (LJZZ212410154030).

Data Availability Statement: Data are contained within the article.

Conflicts of Interest: The authors declare no conflicts of interest.

References

1. Guo, M.; Yang, L.; Son, H.; Le, D.K.; Manickam, S.; Sun, X.; Yoon, J.Y. An Overview of Novel Geometrical Modifications and Optimizations of Gas-Particle Cyclone Separators. *Sep. Purif. Technol.* **2024**, *329*, 125136. [CrossRef]

2. Mengmei Lu, Z.P. Research Progress On the Influence of Structural and Operating Parameter on the Enhanced Separation Performance of Mini-Hydrocyclones. *Chem. Eng. Res. Des.* **2024**. [CrossRef]
3. Li, W.; Huang, Z.; Li, G. Improvement of the Cyclone Separator Performance by the Wedge-Shaped Roof: A Multi-Objective Optimization Study. *Chem. Eng. Sci.* **2023**, *268*, 118404. [CrossRef]
4. Demir, S. A Practical Model for Estimating Pressure Drop in Cyclone Separators: An Experimental Study. *Powder Technol.* **2014**, *268*, 329–338. [CrossRef]
5. Xiong, Z.; Ji, Z.; Wu, X. Development of a Cyclone Separator with High Efficiency and Low Pressure Drop in Axial Inlet Cyclones. *Powder Technol.* **2014**, *253*, 644–649. [CrossRef]
6. Erdal, F.M.; Shirazi, S.A. Local Velocity Measurements and Computational Fluid Dynamics (Cfd) Simulation of Swirling Flow in a Cylindrical Cyclone Separater. *Eng. Technol. Conf. Energy* **2001**, *4*, 326–333.
7. Long, S.; Yang, X.; Yang, J.; Li, B.; Shi, W.; Sommerfeld, M. Euler-Euler Les of Bubble Column Bubbly Flows by Considering Sub-Grid Scale Turbulent Dispersion Effect on Modulating Bubble Transport. *Chem. Eng. J.* **2023**, *477*, 147239. [CrossRef]
8. Zhang, Y. Cfd Study of a Sudden-Expanding Coal Combustor Using Euler–Euler. *Fuel* **2010**, 3643–3649. [CrossRef]
9. Bu, T.; Mesa, D.; Pukkella, A.K.; Brito-Parada, P.R. Optimising Miniaturised Hydrocyclones for Enhanced Separation of Microplastics. *Chem. Eng. J.* **2024**, *496*, 153718. [CrossRef]
10. Elsayed, K.; Lacor, C. Optimization of the Cyclone Separator Geometry for Minimum Pressure Drop Using Mathematical Models and Cfd Simulations. *Chem. Eng. Sci.* **2010**, *65*, 6048–6058. [CrossRef]
11. Wasilewski, M.; Brar, L.S. Effect of the Inlet Duct Angle on the Performance of Cyclone Separators. *Sep. Purif. Technol.* **2019**, *213*, 19–33. [CrossRef]
12. Safikhani, H.; Mehrabian, P. Numerical Study of Flow Field in New Cyclone Separators. *Adv. Powder Technol.* **2016**, *27*, 379–387. [CrossRef]
13. Oka, Y.I.; Okamura, K.; Yoshida, T. Practical Estimation of Erosion Damage Caused by Solid Particle Impact. *Wear* **2005**, *259*, 95–101. [CrossRef]
14. Sedrez, T.A.; Decker, R.K.; da Silva, M.K.; Noriler, D.; Meier, H.F. Experiments and Cfd-Based Erosion Modeling for Gas-Solids Flow in Cyclones. *Powder Technol.* **2017**, *311*, 120–131. [CrossRef]
15. Dehdarinejad, E.; Bayareh, M. Impact of Non-Uniform Surface Roughness on the Erosion Rate and Performance of a Cyclone Separator. *Chem. Eng. Sci.* **2022**, *249*, 117351. [CrossRef]
16. Mirzaei, M.; Clausen, S.; Wu, H.; Nakhaei, M.; Zhou, H.; Jønck, K.; Jensen, P.A.; Lin, W. Investigation of Erosion in an Industrial Cyclone Preheater by Cfd Simulations. *Powder Technol.* **2023**, *421*, 118424. [CrossRef]
17. Zhang, L.; Fan, J.; Zhang, P.; Gao, F.; Chen, G.; Li, J. Effect of Local Erosion on the Flow Field and Separation Performance of the Cyclone Separator. *Powder Technol.* **2023**, *413*, 118007. [CrossRef]
18. Zhao, F.; Chen, Y.; Liu, W.; Xu., D. Experimental Study of the Effect of Different Forms of Deflectors on Cyclone Performance. *Silicate Bulletin* **2007**, *26*, 242–246. [CrossRef]
19. Ji, R.; Zhao, Q.; Zhao, L.; Liu, Y.; Jin, H.; Wang, L.; Wu, L.; Xu, Z. Study On High Wear Resistance Surface Texture of Electrical Discharge Machining Based on a New Water-in-Oil Working Fluid. *Tribol. Int.* **2023**, *180*, 108218. [CrossRef]
20. Zhang, Z.; Yan, S.; Dong, S.; Dong, K.; Zhang, Y.; Wang, B. Study of the Short-Circuit Flow and Circulation Flow'S Impact on Separation Performance of Cyclone Separator with Volute-Helical Inlet. *Adv. Powder Technol.* **2024**, *35*, 104281. [CrossRef]
21. Zandie, M.; Kazemi, A.; Ahmadi, M.; Moraveji, M.K. A Cfd Investigation into the Enhancement of Down-Hole De-Oiling Hydro Cyclone Performance. *J. Pet. Sci. Eng.* **2021**, *199*, 108352. [CrossRef]
22. Zhang, Y.; Reuterfors, E.; McLaury, B.; Shirazi, S.; Rybicki, E. Comparison of Computed and Measured Particle Velocities and Erosion in Water and Air Flows. *Wear* **2007**, *263*, 330–338. [CrossRef]
23. Cao, M.-Q.; Chen, J.-Y.; Hu, B.; Meng, H.; Li, S.-Y.; Wei, Y.-D. Experimental Study on Flow Characteristics of Ash Band in a Cyclone Separator Using Hpiv Techniques. *Sep. Purif. Technol.* **2024**, *337*, 126437. [CrossRef]
24. Xu, Z.; Wang, M.; Chang, L.; Pan, K.; Shen, X.; Zhong, S.; Xu, J.; Liu, L.; Li, G.; Chen, L. Assessing the Particulate Matter Emission Reduction Characteristics of Small Turbofan Engine Fueled with 100% Hefa Sustainable Aviation Fuel. *Sci. Total Environ.* **2024**, *945*, 174128. [CrossRef]
25. Wang, B.; Xu, D.; Chu, K.; Yu, A. Numerical Study of Gas–Solid Flow in a Cyclone Separator. *Appl. Math. Model.* **2006**, *30*, 1326–1342. [CrossRef]